SURFACE DAMAGE OF OXIDIZED METAL MATRIX COMPOSITE LAMINATES UNDER TRANSVERSE TENSION

Dimitris C. Lagoudas, Xinzheng Ma and Shouze Xu

Center for Mechanics of Composites

Department of Aerospace Engineering

Texas A&M University

College Station, TX 77843-3141

ABSTRACT

The oxidation effects on surface crack development of oxidized Ti-15-3 and β-21S Metal Matrix Composite (MMC) unidirectional laminates under applied transverse tension loading are investigated in the present study. An approximate mechanical model is established and a stress analysis of an oxidized laminate with surface cracks is performed. To simplify the analysis, motivated by experimental observations, a periodic distribution of surface cracks in the oxide layer is assumed. The critical value of the applied mechanical load, which is necessary for the formation of new cracks as a function of crack density, is calculated for given oxide layer thickness. The effective stiffness reduction, caused by the formation of the surface cracks, is also evaluated. Finally, the influence of gradient effective properties of the metal matrix underneath the oxide layer, caused by the diffusion of oxygen, on the stress field is considered.

1. INTRODUCTION

Titanium alloy Metal Matrix Composites (MMC) are rapidly becoming the choice of aerospace engineers because of their high strength, low density and ability to retain mechanical integrity at relatively high temperatures. Applications anticipated for structural components in advanced turbine engines and hypersonic aircraft require the structural composite to withstand severe mechanical loading and temperature variations.

Oxidation has been shown experimentally to significantly contribute to damage development in titanium MMC systems at elevated temperatures (Gabb et al. 1991, Lerch et al. 1990, Bartolotta and Verilli 1992, Revelos and Smith 1992, Allen et al. 1994, Lagoudas et al. 1995). Oxidation severely degrades the composite when a brittle oxide layer on the titanium alloy develops. This oxide layer initiates and accelerates damage throughout the composite. Our own preliminary studies of surface oxidation on SiC/Ti-15-3 MMC unidirectional laminates verifies the formation of a brittle TiO_2 layer (Lagoudas et al. 1995).

A series of experiments were performed to determine the thickness of the oxide layer formed on the surface of Ti-15-3, Ti-β21S and commercially pure titanium exposed to temperatures of 600°C to 800°C. Several of the oxidized specimens were then loaded at

room temperature under tensile stress. Fig. 1 is a surface view of a specimen (with cross section 3.2mm by 0.68mm) of commercially pure titanium exposed to air at 700°C for 10 hours and loaded to a tensile force of 570N. The developed oxide layer thickness is 5 μm. The darker blocks are areas where the oxide layer has peeled off of the metal. From the figure, the development of surface cracks appears to follow a regular periodic pattern. This observation will be used in the sequel for the mechanical stress analysis model. We will also use elastic analysis, because the mechanical load is applied at room temperature and the damage occurs at low stress levels.

For the stress analysis of composite laminates with periodic cracks, a model first developed by Hashin (1985) for an approximate evaluation of the stress field and stiffness reduction is utilized. Kaveh-Ahangar (1990) and Varna and Berglund (1991), among others, further developed this model with more general forms of test stress functions. In the present work, both polynomial and exponential stress functions are investigated, to model the stress state in a unidirectional MMC oxidized laminate under applied in-plane transverse tensile load, with periodic surface cracks.

Section 2 outlines the statement of the problem and the solution procedure. In Section 3, the critical value of mechanical load is calculated for the creation of new surface cracks as a function of crack density for given oxide layer thickness. The effective stiffness reduction due to cracks caused by the oxidation process is also evaluated. The effect of oxidation induced eigenstrains is taken into account in the mechanical analysis, and the evolution of crack density for different eigenstrains is estimated as a function of the applied loading. Section 4 discusses the effect of the stiffness gradation in the metal matrix due to the change in the microstructure caused by oxygen diffusion. Finally, conclusions are given in Section 5.

2. Approximate Stress Analysis for a MMC Laminate with Surface Cracks

Fig. 2(a) shows the schematic of a cross section of an oxidized MMC laminate, subsequently damaged by an applied mechanical load. The total thickness of the laminate is denoted by $2h$, while the thickness of each of the oxide layers is b. It is assumed that the surface cracks are periodically distributed along the laminate in the direction of an applied transverse in-plane load, $2N_{11}$(force/length). Due to the periodicity and symmetry of the mechanical problem, we only need to solve it in a unit cell, as shown in Fig. 2(b). For convenience, the origin of the coordinate system is set at the center of the material surface between two adjacent cracks. The stress field in each material, i.e. oxide and the remaining composite, is obtained by superposition of the stress fields of two auxiliary problems (Hashin, 1985)

$$\sigma_{ij}^{t(p)} = \sigma_{ij}^{o(p)} + \sigma_{ij}^{(p)}, \tag{1}$$

where $p = 1$ for the oxide layer, and $p = 2$ for the unoxidized composite domain. The left side of the equation represents the total stress field, and the two terms on the right hand side are the stresses for the first and second auxiliary problems, respectively, defined in the next

paragraph.

The first auxiliary problem is similar to the original problem except that there are no surface cracks, while the external load is applied. This is a simple elasticity problem and the solution can be easily obtained as

$$\sigma_{11}^{o(1)} = \sigma_1 , \qquad \sigma_{11}^{o(2)} = \sigma_2 \tag{2}$$

where σ_1 and σ_2 are constants. All other stresses are zero. The second auxiliary problem has the same geometry with the original one, but the surfaces of the cracks are subjected to an applied traction such that upon superposition of the stress fields in the two auxiliary problems, traction free crack surfaces are achieved and the externally applied load is recovered.

In what follows, the main effort will be made to obtain the solution for the second auxiliary problem which involves the assumption and determination of a class of admissible Airy stress functions. For the second auxiliary problem, we therefore assume the Airy stress functions to be of the following type:

$$\begin{aligned} \Phi^{(1)}(x_1, x_2) &= \phi_1(x_1)\ \psi_1(x_2), && 0 \le x_2 < b \\ \Phi^{(2)}(x_1, x_2) &= \phi_2(x_1)\ \psi_2(x_2), && b \le x_2 \le h \end{aligned} \tag{3}$$

where $\phi_1(x_1)$, $\phi_2(x_1)$, $\psi_1(x_2)$ and $\psi_2(x_2)$ are unknown functions to be determined. The expressions for the stress components in terms of the stress functions defined above are:

$$\sigma_{11}^{(1)} = \phi_1(x_1)\psi''_1(x_2), \quad \sigma_{12}^{(1)} = -\phi'_1(x_1)\psi'_1(x_2), \quad \sigma_{22}^{(1)} = \phi''_1(x_1)\psi_1(x_2) \tag{4}$$

and

$$\sigma_{11}^{(2)} = \phi_2(x_1)\psi''_2(x_2), \quad \sigma_{12}^{(2)} = -\phi'_2(x_1)\psi'_2(x_2), \quad \sigma_{22}^{(2)} = \phi''_2(x_1)\psi_2(x_2) \ . \tag{5}$$

where $(')$ denotes first derivative and $('')$ denotes second derivative with respect to the independent variable. From global equilibrium in x_1 direction it follows

$$\phi_2(x_1) = \lambda\phi_1(x_1) \tag{6}$$

where $\lambda = -[\psi'_1(b) - \psi'_1(0)] / [\psi'_2(h) - \psi'_2(b)]$ is a constant. Eq.(6) indicates the dependence between $\phi_1(x_1)$ and $\phi_2(x_1)$ and therefore reduces the number of unknown functions from four to three.

The traction boundary conditions along x_1 result in the following requirements for the stress components for the second auxiliary stress problem:
at $x_2 = 0$ (free surface),

$$\sigma_{12}^{(1)}(x_1,0) = 0, \quad \sigma_{22}^{(1)}(x_1,0) = 0 \tag{7}$$

at $x_2 = b$ (oxide metal interface),

$$\sigma_{12}^{(1)}(x_1,b) = \sigma_{12}^{(2)}(x_1,b), \quad \sigma_{22}^{(1)}(x_1,b) = \sigma_{22}^{(2)}(x_1,b) \tag{8}$$

and at $x_2 = h$ (mid-plane of laminate),

$$\sigma_{12}^{(2)}(x_1,h) = 0. \tag{9}$$

From the conditions imposed by Eq. (7) , (8) and (9) , respectively, it follows that

$$\begin{aligned} &\psi_1(0) = 0, \qquad \psi'_1(0) = 0 \\ &\psi_1(b) = \lambda\psi_2(b), \quad \psi'_1(b) = \lambda\psi'_2(b) \\ &\psi'_2(h) = 0. \end{aligned} \tag{10}$$

The remaining traction boundary conditions at $x_1 = \pm a$, result in:

$$\begin{aligned} &\sigma_{11}^{(1)}(\pm a, x_2) = -\sigma_1, \qquad 0 \le x_2 \le b \\ &\sigma_{12}^{(1)}(\pm a, x_2) = 0, \qquad 0 \le x_2 \le b. \end{aligned} \tag{11}$$

The requirements imposed on the unknown functions by the above boundary conditions, respectively, are:

$$\phi_1(\pm a)\psi''_1(x_2) = -\sigma_1, \quad 0 \le x_2 \le b; \qquad \phi'_1(\pm a) = 0. \tag{12}$$

Without losing generality, from the first condition above one can derive:

$$\phi(\pm a) = 1; \qquad \psi''_1(x_2) = -\sigma_1, \quad 0 \le x_2 \le b. \tag{13}$$

To satisfy the second condition of Eq. (13) and the first and second conditions of Eq.(10), we have:

$$\psi_1(x_2) = -\frac{\sigma_1}{2}x_2^2. \tag{14}$$

For the test function $\psi_2(x_2)$ the last three conditions of Eq. (10) have to be met. In the present work two different test functions are investigated that satisfy these boundary conditions:

i) exponential form

$$\psi_2^e(x_2) = \frac{\sigma_1 b}{1-e^{-kc}}[1/k(e^{-k(x_2-b)}-1)+e^{-kc}(x_2-b/2)-b/2], \tag{15}$$

ii) polynomial form

$$\psi_2^p(x_2) = \sigma_1 b[-\frac{b}{2}-(x_2-b)+\frac{(x_2-b)^{2-k}c^{k-1}}{k(2-k)}-\frac{(1-k)(x_2-b)^2}{2kc}]. \tag{16}$$

In the above k is a parameter to be determined. After the test function $\psi_2(x_2)$ is selected, the only remaining unknown function is $\phi_1(x_1)$ and the parameter k. To find $\phi_1(x_1)$ and k, the principle of minimum complementary energy is employed, for the second auxiliary problem (Hashin, 1985). The total complementary energy of the composite system with the oxide layer for the second auxiliary problem is given by

$$U[\phi_1(x_1);\ k] = \frac{1}{2}\int_{-a}^{a}[C_{00}\phi_1^2(x_1)+C_{02}\phi_1(x_1)\phi''_1(x_1)+C_{11}\phi'^2_1(x_1)+C_{22}\phi''^2_1(x_1)]dx_1 \tag{17}$$

where,

$$
\begin{aligned}
C_{00} &= \int_0^b \frac{1}{E_o}[\psi''_1(x_2)]^2\ dx_2 + \int_b^{b+c} \frac{1}{E_m}[\psi''_2(x_2)]^2 dx_2 \\
C_{02} &= -2\nu_o \int_0^b \frac{1}{E_o}[\psi''_1(x_2)\psi_1(x_2)]\ dx_2 - 2\nu_m \int_b^{b+c} \frac{1}{E_m}[\psi''_2(x_2)\psi_2(x_2)]dx_2 \\
C_{11} &= \int_0^b \frac{2(1+\nu_o)}{E_o}[\psi'_1(x_2)]^2\ dx_2 + \int_b^{b+c} \frac{2(1+\nu_m)}{E_m}[\psi'_2(x_2)]^2 dx_2 \\
C_{22} &= \int_0^b \frac{1}{E_o}[\psi_1(x_2)]^2\ dx_2 + \int_b^{b+c} \frac{1}{E_m}[\psi_2(x_2)]^2 dx_2
\end{aligned}
\tag{18}
$$

and E_o, ν_o and E_m,ν_m are the elastic Young's moduli and Poisson's ratios for the oxide layer and the remaining composite region, respectively. Explicit evaluations for the constants C_{00}, C_{02}, C_{11}, C_{22} are given in Appendix 1 for both the exponential and the polynomial cases. The Euler-Lagrange equation for $\phi_1(x_1)$ necessary for a stationary value of U is found to be

$$\phi''''_1(x_1) + p\,\phi''_1(x_1) + q\,\phi_1(x_1) = 0 \tag{19}$$

where $p=(C_{02}-C_{11})/C_{22}$, $q=C_{00}/C_{22}$ and $(''''')$ denotes fourth derivative withe respect to independent variable . The solution of the above ordinary differential equation is of the form $\phi_1(x_1)=\sum_{i=1}^{4} A_i e^{s_i x_1}$, where s_i are the roots of the characteristic equation

$$s^4 + ps^2 + q = 0. \tag{20}$$

The constants A_i are evaluated by using the first condition of Eq.(13) and the second condition of Eq.(12). Explicit evaluations for the constants are given in Appendix 2. After the function $\phi_1(x_1)$ is determined the complementary energy is expressed as function of the only unknown parameter left, *k*. To determine this last unknown parameter, the condition

$$\frac{\partial U[\phi_1(x_1);k]}{\partial k} = 0 \tag{21}$$

has been used. In present work the value of k has been found numerically from the graph of U.

3. MMC Oxidized Cracked Laminates with Uniform Effective Properties

As an example we deal with a four-ply unidirectional MMC with Ti-15-3 matrix and SiC fibers. Table 1 gives the individual phase properties used in this study for the Ti-15-3 system as well as the Mori-Tanaka approximation to the effective laminate properties. In fact, the composite consists of three different phases, namely, fibers, matrix and oxide. Although all the individual phases are isotropic materials, the fiber geometry and orientation makes the composite anisotropic. In view of the unidirectional and uniformly distributed fibers in the matrix, one may regard the unoxidized composite as statistically homogeneous and transversely isotropic in a macroscopic scale. Therefore, for the purpose of this study, we assume two material regions: an isotropic oxide layer on the surface, and an effective transversely isotropic MMC. Those effective material properties are functions of fiber volume fraction and individual phase (matrix and fiber) properties and are computed for the composite laminate using the Mori-Tanaka averaging scheme (Lagoudas, et al. 1991).

Table 1 Thermoelastic constituent mechanical properties

	E (GPa)	ν
Ti-15-3	92.39	0.32
TiO_2	282.585	0.28
SiC fiber	413.7	0.20
MMC (transverse)	138.6	0.35

The computed value for k corresponding to the minimum energy is 0.175/μm in the exponential case (a) and 0.397 in the polynomial case (b) for material properties given in Table 1 and the values of the geometric parameters shown in Fig. 2 assume to be 2a=600μm, b=5μm, c=300μm for fiber volume fraction c_f =0.32.

The stress components are computed as functions of position both in the x_1 and x_2 (the applied load) directions. Fig.3 is a plot of the normal stress, $S_{11} = \sigma_{11} h / N_{11}$ vs. the position at $x_1 = a$. The finite element method (FEM) result is also shown in the figures for comparison. It can be seen that the stress increases sharply when approaching the crack tip and asymptotically goes to a constant far away from the tip. The polynomial result is a better approximation for the FEM result. Fig.4 shows a comparison of the normal stresses $S_{11} = \sigma_{11} h / N_{11}$ in the oxide layer. Obviously the stress distribution assumptions used in this study are better descriptions of the stress concentration at the crack tip than a uniform (Hashin, 1985), linear(Kaveh-Ahangar, 1990) or non-singular hyperbolic(Varna and Berglund, 1991) stress distribution assumption.

Table 2 The values of *k* from the principle of total complementary energy

b	*k*	b	*k*	b	*k*
30	0.187	2.5	0.436	0.01	0.495
20	0.260	1.0	0.457	0.001	0.498
10	0.344	0.5	0.470	0.0005	0.499
5	0.397	0.1	0.486		

Table 2 gives some values of *k* vs. crack size b holding a and c constant. The limit of the value of *k* for the polynomial case when the ratio of b/a approaches to 0 is 0.5, which is identical to the conclusion of fracture mechanics.

The cracks in the oxide layer reduce the stiffness of the material, and allow the material damage to occur more easily. The reduction generally depends on the crack density. To investigate the damage procedure, the effective stiffness is evaluated by means of the energy method.

The complementary energy for the effective medium under tension σ^* is

$$U_{eff} = \frac{1}{2}\frac{\sigma^{*2}}{E_{eff}}V \tag{22}$$

where E_{eff} is the axial effective Young's modulus for the medium, and V is the volume of the RVE. The complimentary energy of the undamaged material is given by

$$U^o = \frac{1}{2}\frac{\sigma^{*2}}{E^o}V \tag{23}$$

where E^o is the axial effective Young's modulus for the undamaged medium. According to the principle of complementary energy, we have for the damaged medium

$$U_{eff} \le U^o + U \tag{24}$$

where U is in terms of the admissible stress system, Eq.(18). Combining Eq.(24) with Eqs.(22) and (23), gives the following bound for the effective Young's modulus:

$$\frac{1}{E_{eff}} \leq \frac{1}{E^{o}} + \frac{2U}{V\sigma^{*2}}. \tag{25}$$

The normalized effective Young's modulus, from both this model and FEM, has been plotted against crack density in Fig.5. It can be seen that when the crack density reaches a certain value (0.8 in this case), the modulus has a significant reduction of up to 14%.

The maximum normal stress in the loading direction has the following value

$$\sigma_{11}^{t(1)}(0, x_2) = \frac{E_o N_{11}}{bE_o + cE_m}[1 - \phi_1(0)]. \tag{26}$$

By application of the fracture criterion, a new crack will be initiated at the location where the normal stress in the oxide reaches a critical value, σ_{cr}, which may be stated as

$$\sigma_{11}^{t(1)}(0, x_2) = \sigma_{cr}. \tag{27}$$

In view of Eq.(27), Eq.(26) may be rewritten as

$$N_{11} = \frac{bE_o + cE_m}{E_o[1 - \phi_1(0)]}\sigma_{cr}. \tag{28}$$

This expression describes the relationship between the applied load and the crack density. From this relationship, one may find either the crack density under given load condition or the load necessary, at a given crack density, to create a new crack in the oxide layer.

Because of the phase transformation from Ti-15-3 into titanium oxide and the CTE mismatch between the two materials, an eigenstrain , ε_{11}^{tr}, was introduced in the oxide layer. To include this effect into this study, we need to solve the corresponding eigenstress problem. Considering the RVE in Fig.2, assume that there are no external forces or displacement constraints, and only the internal eigenstrain exists in the oxide layer. Assuming that the total strain ε_{11} is constant, the normal stresses in the x_1 direction takes the form:

$$\sigma_{11}^{tr(1)} = E_o(\varepsilon_{11} - \varepsilon_{11}^{tr}) , \qquad \sigma_{11}^{tr(2)} = E_m \varepsilon_{11} \tag{29}$$

while equilibrium of forces requires

$$\int_0^b \sigma_{11}^{tr(1)} dx_2 + \int_b^h \sigma_{11}^{tr(2)} dx_2 = 0. \tag{30}$$

If we solve Eqs.(29) and (30), the normal stress in the oxide layer is obtained as

$$\sigma_{11}^{tr(1)} = -\frac{cE_oE_m}{bE_o+cE_m}\,\varepsilon_{11}^{tr}. \tag{31}$$

Since the titanium oxide has a larger CTE than that of Ti-15-3, the eigenstress in the oxide layer is compressive.

The total normal stress in the x_1 direction in the oxide layer can be obtained by adding the eigenstress, Eq.(31), to Eq.(26). Consequently, the relationship between the applied load and the critical stress for the generation of new cracks, i.e., Eq.(28) becomes

$$N_{11} = \frac{bE_o+cE_m}{E_o[1-\phi_1(0)]}\sigma_{cr} + \frac{cE_m\varepsilon_{11}^{tr}}{[1-\phi_1(0)]}. \tag{32}$$

It can be seen that the eigenstrain plays a role of mechanical toughening in the oxide layer. For example, if the eigenstrain is 0.1%, then it will cause an eigenstress of as much as -272Mpa for the materials and configuration used in this study. The significant reduction of tensile stress greatly delays the generation and development of new cracks.

4. MMC Laminate with Surface Cracks and Gradient Effective Properties

Although the oxidation resistant Ti-β21S alloy forms a much thinner oxide layer than Ti-15-3, after similar exposure to the oxidizing environment, it is necessary to investigate the surface damage of the Ti-β21S alloy. This is because the oxide layer has a larger Young's modulus than the titanium alloy (Shackelford et al. 1994), which will cause stress concentration, and a lower fracture critical strength, which will cause new cracks in the oxidized specimen at a lower level of stress than in the specimen of the net alloy itself.

When the β-21S alloy is used as the matrix in a MMC in a high temperature environment, the phase transformation is not uniform. Instead, the individual material phases are functions of position. However, the formation of a brittle alpha enriched zone below the oxide layer, shown in Fig. 6 for oxidation at 700°C for 72 hours, is responsible for the final propagation of surface cracks into the composite laminate under mechanical loading. In such cases, the overall material properties in general are also functions of position. Therefore in using the variational approach, the formulation for the mechanical modeling will be different from what has been discussed for materials like Ti-15-3 in previous sections of this study.

The result for the first auxiliary problem, namely, the stress is no longer uniform in the region where the properties are not uniform. Suppose the Young's modulus in the metal substrate varies with thickness and is denoted as $E_2(x_2)$, then instead of using Eq.(2), the stresses for this problem are given by:

$$\sigma_{11}^{o(1)} = \frac{E_1}{bE_1 + c\overline{E}_2} N$$
$$\sigma_{11}^{o(2)} = \frac{E_2(x_2)}{bE_1 + c\overline{E}_2} N \tag{33}$$

where

$$\overline{E}_2 = \frac{1}{c} \int_b^h E_2(w)dw. \tag{34}$$

Due to the fact that the solution of the first auxiliary problem is a function of position, x_2, the evaluation for other stress components via integration of equilibrium equations will become more complex. However, the procedure for solving the problem and most of the expressions remain the same, and the material properties are now functions of position.

As an example, a recently developed β-Ti titanium alloy material, β-21S, is to be considered for the dependence of its Young's modulus on the location. Wallace, et al.(1993) investigated the effect of oxidation on the mechanical properties of β-21S at temperatures of 600°C, 700°C and 800°C. It was found that the tensile strength and elastic modulus were degraded by the oxidation exposure. The microstructure of the material changes with the oxygen concentration which in turn changes with position. Particularly for the 800°C case, the increased oxygen content causes the formation of grain boundary α phase as well as the precipitation of α in the interior of the β grains near the surface where the oxygen concentration is highest. In another paper (Wallace, et al. 1990), an experimental result was obtained for the α Ti content as a function of distance from the oxide/metal interface for β-21S exposed at 800°C. The α-Ti concentration, c_α can be given as a exponential function of the distance from the oxide/metal interface into the metal by means of curve fitting. Since the microstructures of α-Ti and β-Ti are different from each other, so are their material properties. Therefore, if the concentrations of individual phases are functions of position, then the effective properties are also functions of position.

If E_α and E_β are Young's moduli of α-Ti and β-Ti, respectively, then the effective property $_{\alpha\beta}$ will depend on $c_\alpha(w)$, in addition to the individual moduli of the two phases. While the value of E_β can be obtained from the literature (Wallace, et al. 1993), E_α is not available. However, one may find the average value of $E_{\alpha\beta}$ from experiments (Wallace, et al. 1993), i.e.

$$\overline{E}_{\alpha\beta} = \frac{1}{c} \int_b^{b+c} E_{\alpha\beta}(w)dw. \tag{35}$$

Thus, by integrating both sides of Eq.(35) together with the two determined properties, one may get the equation from which the value of E_α can be found. Table 3 gives the values of Young's moduli for β-21S exposed at 800°C for 30 hours.

Table 3 Young's moduli for β-21S at 800°C

E_α	E_β	$\overline{E}_{\alpha\beta}$
182.8 GPa	69 GPa	89.3 GPa

Here E_β and $\overline{E}_{\alpha\beta}$ are taken from Wallace's experiment (Wallace, et al. 1993). The value of E_α can be determined by means of the law of mixture which has the following form:

$$E_\alpha = \frac{\overline{E}_{\alpha\beta} - (1-\overline{c}_\alpha)\ E_\beta}{\overline{c}_\alpha}. \tag{36}$$

The Mori-Tanaka approach (Weng, 1984) has also been used for the evaluation of effective properties. The scheme can be briefly described as following:

$$\boldsymbol{L} = \boldsymbol{L}_\beta + c_\alpha(\boldsymbol{L}_\alpha - \boldsymbol{L}_\beta)\boldsymbol{A}_\alpha \tag{37}$$

where $\boldsymbol{L}$ denotes the effective stiffness matrix, $\boldsymbol{L}_\alpha$ and $\boldsymbol{L}_\beta$ are stiffness matrices for α-Ti and β-Ti, respectively. $\boldsymbol{A}_\alpha$ is the strain concentration matrix which is given by

$$\boldsymbol{A}_\alpha = [\boldsymbol{I} + c_\beta\ \boldsymbol{S}\boldsymbol{L}_\beta^{-1}(\boldsymbol{L}_\alpha - \boldsymbol{L}_\beta)]^{-1}$$

(Lagoudas, et al. 1991), where $\boldsymbol{I}$ is the identity matrix and $\boldsymbol{S}$ is the Eshelby tensor for a sphere (Mura, 1987). Here we use a spherical shape for the Eshelby tensor because of the fine particles of α-Ti phase embedded in β-Ti phase, which can be seen from the experiment (Fig.6).

Fig.7 gives two estimates of the effective Young's modulus based on the rule of mixtures and the Mori-Tanaka approach. It can be seen that although the former does not include factors such as Poisson's ratio and the shape of individual phases as the latter does, they give close results.

The stress field has been evaluated for the MMC with non-uniform properties, and compared to the uniform properties case. In Fig.8 the normalized stress, $S_{11} = \sigma_{11}/(N_{11}/h)$, for both cases has been plotted along the cross-section of the RVE at x_1=a. It is obvious that the stress increases substantially in the region close to the interface due to the material properties change.

5. CONCLUSIONS

For the stress approximation in the cracked MMC, both the variational approaches with the exponential and polynomial assumptions provide simple yet quite accurate

approximations of the stiffness. The latter are better in the composite near the crack. The polynomial assumption gives the power of singularity which is identical to the theoretical results when the size of the crack is infinitely small. The FEM results have also displayed a favorable comparison.

Although the titanium dioxide layer (rutile) has a larger stiffness than that of the MMC, it can not sustain much tensile loading. Consequently, it breaks very easily under tension and thus causes overall stiffness reduction. An estimation of stiffness reduction as a function of crack density has been obtained and the result shows that the reduction is significant for thick oxide layers.

Metallic matrix materials such as β-21S display non-uniform mechanical properties after oxidation. In such cases, the stress field can still be obtained from a modified approximate model. The difference between the material systems with uniform properties and non-uniform properties is substantial, particularly at places close to the oxide/matrix interface where the stiffness in the matrix reaches the highest value.

ACKNOWLEDGMENTS

The authors acknowledge the support of AFOSOR grant No.F49620-94-1-0341.

REFERENCES

Allen, D.H., Eggleston, M.R., and Hurtado, L.D., "Recent Research on Damage Development in SiC/Ti Continuous Fiber Metal Matrix Composites," to appear in *Fracture of Composites*, E.A. Armanios (ed.), in *Key Engineering Materials* series, Trans Tech Publications, 1994.

Bartolotta, P., and Verrilli, M.J., "Thermomechanical Fatigue Behavior of SiC/Ti-24Al-11Nb in Air and Argon Environments," *NASA TM-105723*, 1992.

Gabb, T.P., Gayda, J., and MacKay, R.A., "Nonisothermal Fatigue Degradation of a SiC/Ti Composite," *Ceramic Transactions*, Vol. 19, 1991, pp. 527-534.

Hashin, Z., "Analysis of Cracked Laminates: A Variational Approach," *Mechanics of Materials*, Vol. 4, 1985, p. 121.

Kaveh-Ahangar, A. "Analysis of Progressive Damage in Fibrous Composite Laminates," *Ph. D. Thesis, Rensselaer Polytechnic Institute*, 1990.

Jansson, S., Dève, H.E., and Evans, A.G., "The Anisotropic Mechanical Properties of a Ti Matrix Composite Reinforced with SiC Fibers," *Metallurgical Transactions A*, Vol. 22A, 1991, pp. 1991-2975.

Lagoudas, D.C., Gavazzi, A.C., and Nigam, H., "Elastoplastic Behavior of Metal Matrix Composites Based on Incremental Plasticity and the Mori-Tanaka Averaging Scheme," *Computational Mechanics*, Vol. 8, 1991, pp. 193-203.

Lagoudas, D.C., Ma, X., Miller, D.A. and Allen, D.H., "Modeling of Oxidation in Metal Matrix Composites," *Int. J. Engng Sci*., Vol. 33, No. 15, 1995, pp. 2327-2343.

Laws,N. and Dvorak, G. J., "Progressive Transverse Cracking in Composites Laminates," *J. Composite Materials*, Vol.22, p.900 (1988).

Lerch, B.A., Gabb, T.P., and MacKay, R.A., "Heat Treatment Study of the SiC/Ti-15-3 Composite System," *NASA TP-2970*, 1990.

Lissenden, C.J., Herakovich, C.T., and Pindera, M.-J., *Inelastic Deformation of Metal Matrix Composites*, Report AM-93-03, University of Virginia, Charlottesville VA, 1993.

Miller, D.A., "Damage Evolution of a SiC/Ti-15-3 Metal Matrix Composite With Different Heat Treatments," *M.S. Thesis, Texas A&M University*, 1995.

Mura,T., "Micromechanics of Defects in Solids," 2nd edition, Martinus Wijhott, Dordrecht, 1987.

Newaz, G.M., Majumdar, B.S., and Brust, F.W., "Thermal Cycling Response of Quasi-Isotropic Metal Matrix Composites," *J. Engineering Materials and Technology, Transactions of the ASME*, Vol. 114, 1992, pp. 156-161.

Revelos, W.C., and Smith, P.R., "Effect of Environment on the Thermal Fatigue Response of and SCS-6/Ti-24Al-11Nb Composite," *Metallurgical Transactions A*, Vol. 23A, 1992, pp. 587-595.

Shackelford, J.F., Alexander, W., and Park, J.S., "CRC Material Science and Engineering Handbook," CRC Press Inc., 1994, pp.510.

Varna, J. and Berglund, L., "Multiple Transverse Cracking and Stiffness Reduction in Cross-Ply Laminates," *J. Composites Technology & Research*, Vol. 13, 1991, pp. 99-106.

Varna, J. and Berglund, L., "Thermo-Elastic Properties of Composite Laminates with Transverse Cracks," *J. Composites Technology & Research*, Vol. 16, 1994, pp. 77-87.

Wallace, T.A., Clark, R.K., Sankaran, S.N., and Weidemann, K.E., "Oxidation Characteristics of Ti-25Al-10Nb-3V-1Mo Intermetallic Alloy," *NASA TP-304*4, 1990.

Wallace,T.A.,Wiedemann, K.E., and Clark, R.K., "Oxidation Characteristics of Beta-21S in Air in the Temperature Range 600 to 800°C," *NASA Technical Memorandum* 104217,1992.

Wallace,T.A.,Bird, R.K., and Wiedemann, K.E., "The Effect of Oxidation on the Mechanical Properties of Beta-21S," *Beta Titanium Alloys in the 1990's, The Minerals, Metals & Materials Society*, 1993

Weng, G.J., "Some Elastic Properties of Reinforced Solids, with Special Reference to Isotropic Ones Containing Spherical Inclusions," *Int. J. Eng. Sci*., Vol.22, 1984, pp.845-856.

APPENDIX 1

Explicit evaluations for constants defined in Eq. (19):

I).Exponential case:

$$C_{00} = 1/E_o + \int_0^c 1/E_m e^{-2kw} dw$$

$$C_{02} = -\nu_o b^2/3E_o + \int_0^c 2\nu_2/E_m e^{-kw}[(1-e^{-kw})/k - e^{-kc}(w+b/2)+b/2]dw$$

$$C_{11} = 2b^2(1+\nu_o)/3E_o + \int_0^c 2(1+\nu_2)/E_m (e^{-kw}-e^{-kc})^2 dw \qquad \text{(A1-1)}$$

$$C_{22} = b^4/20E_o + \int_0^c 1/E_m [(1-e^{-kw})/k - e^{-kc}(w+b/2)+b/2]^2 dw$$

ii).Polynomial case:

$$C_{00} = 1/E_o + b\int_0^c \frac{1}{E_m}[\frac{(1-\alpha)c^{\alpha-1}}{\alpha}]^2 [w^{-\alpha}-c^{-\alpha}]^2 dw$$

$$C_{02} = -\nu_o b^2/3E_o + b\int_0^c \frac{2\nu_2}{E_m}\frac{(1-\alpha)c^{\alpha-1}}{\alpha}[w^{-\alpha}-c^{-\alpha}]$$
$$[-\frac{b}{2}-w+\frac{w^{2-\alpha}c^{\alpha-1}}{\alpha(2-\alpha)}-\frac{(1-\alpha)w^2}{2\alpha c}]dw \qquad \text{(A1-2)}$$

$$C_{11} = 2b^2(1+\nu_o)/3E_o + b\int_0^c \frac{2(1+\nu_2)}{E_m}[1-\frac{w^{1-\alpha}c^{\alpha-1}}{\alpha}+\frac{(1-\alpha)w}{\alpha c}]^2 dw$$

$$C_{22} = b^4/20E_o + b\int_0^c \frac{1}{E_m}[-\frac{b}{2}-w+\frac{w^{2-\alpha}c^{\alpha-1}}{\alpha(2-\alpha)}-\frac{(1-\alpha)w^2}{2\alpha c}]^2 dw$$

APPENDIX 2

The solusion of (20) is more convenient to be given by using hyperbolic or triangle function forms instead of using exponential form. Here we give:

I). $p^2 < 4q$:

$$\phi_1(x_1) = B_1\cosh(ux_1)\cos(vx_1)+B_2\sinh(ux_1)\sin(vx_1) \qquad \text{(A2-1.a)}$$

where

$$B_1 = \frac{2(u\cosh(ua)\sin(va) + v\sinh(ua)\cos(va))}{u\sin(2va) + v\sin(2ua)},$$

$$B_2 = \frac{2(v\cosh(ua)\sin(va) - u\sinh(ua)\cos(va))}{u\sin(2va) + v\sin(2ua)}, \qquad \text{(A2-1.b)}$$

$$u = q^{1/4}\cos\frac{1}{2}\ ,\ v = q^{1/4}\sin\frac{1}{2}\ ,\quad = arctg((4q/p^2 - 1)^{0.5}).$$

ii). $p^2 \geq 4q,\ p<0$

$$\phi_1(x_1) = B_1\cos(ux_1) + B_2\cos(vx_1) \qquad \text{(A2-2.a)}$$

where

$$B_1 = \frac{v\sin(va)}{v\cos(ua)\sin(va) - u\cos(va)\sin(ua)},$$

$$B_2 = \frac{-u\sin(ua)}{v\cos(ua)\sin(va) - u\cos(va)\sin(ua)}, \qquad \text{(A2-2.b)}$$

$$u = [1/2(|p| + (p^2 - 4q)^{1/2})]^{1/2},\quad v = [1/2(|p| - (p^2 - 4q)^{1/2})]^{1/2}$$

iii). $p^2 \geq 4q,\ p>0$

$$\phi_1(x_1) = B_1\cosh(ux_1) + B_2\cosh(vx_1) \qquad \text{(A2-3.a)}$$

where

$$B_1 = \frac{v\sinh(va)}{v\sinh(va)\cosh(ua) - u\sinh(ua)\cosh(va)},$$

$$B_2 = \frac{-u\sinh(ua)}{v\sinh(va)\cosh(ua) - u\sinh(ua)\cosh(va)}, \qquad \text{(A2-3.b)}$$

$$u = [1/2(|p| + (p^2 - 4q)^{1/2})]^{1/2},\quad v = [1/2(|p| - (p^2 - 4q)^{1/2})]^{1/2}$$

Fig.1 Surface view of commercially pure titanium exposed to air at 700^0C for 10 hrs and subjected to a tensile stress (specimen width $\approx$ 3.2mm);

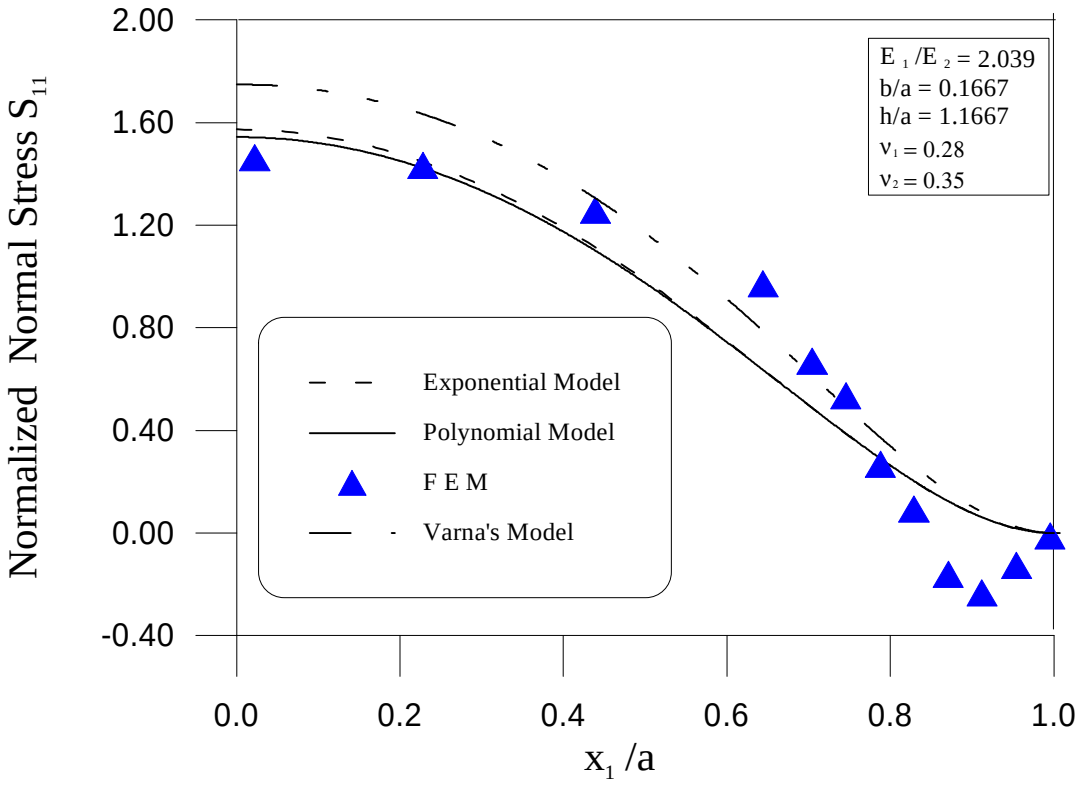

Fig.4(a) Normalized normal stress, $\bar{\sigma}_{11} = \sigma_{11} h/N_1$, on the surface of the oxide layer under the transverse load.

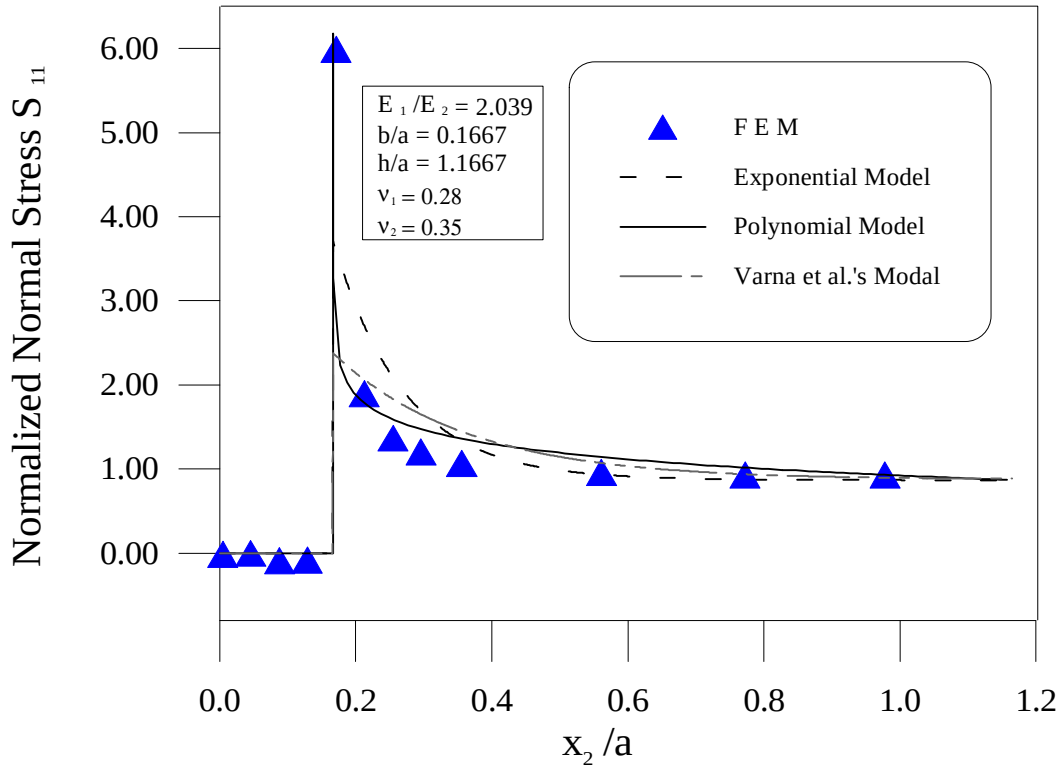

Fig.3(a) The normalized normal stress, $S_{11} = \sigma_{11} h/N_{11}$, through the thickness at $x_1 = a$.

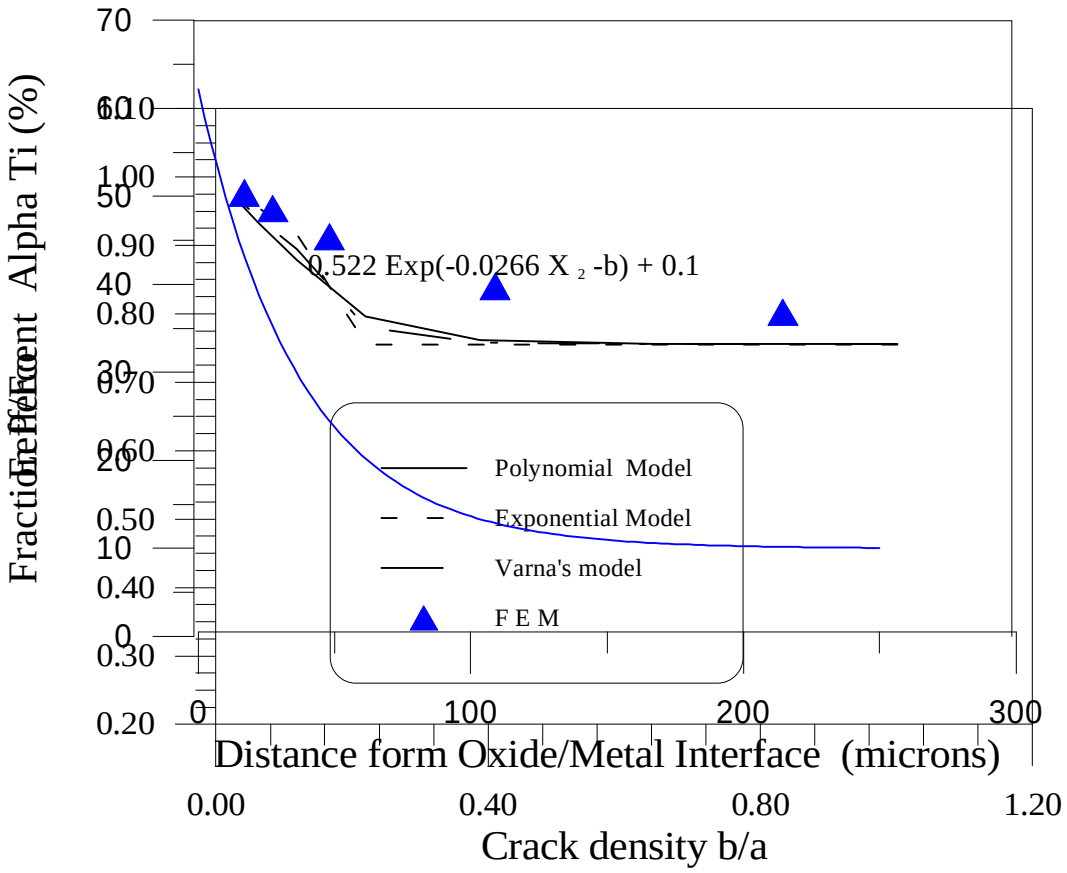

Fig.7 Effective stiffness reduction as a function of crack density (b/a).

Fig.9 Fraction percent of α-Ti as a function of position, based on the experiment (Wallaace, et al., 1992)

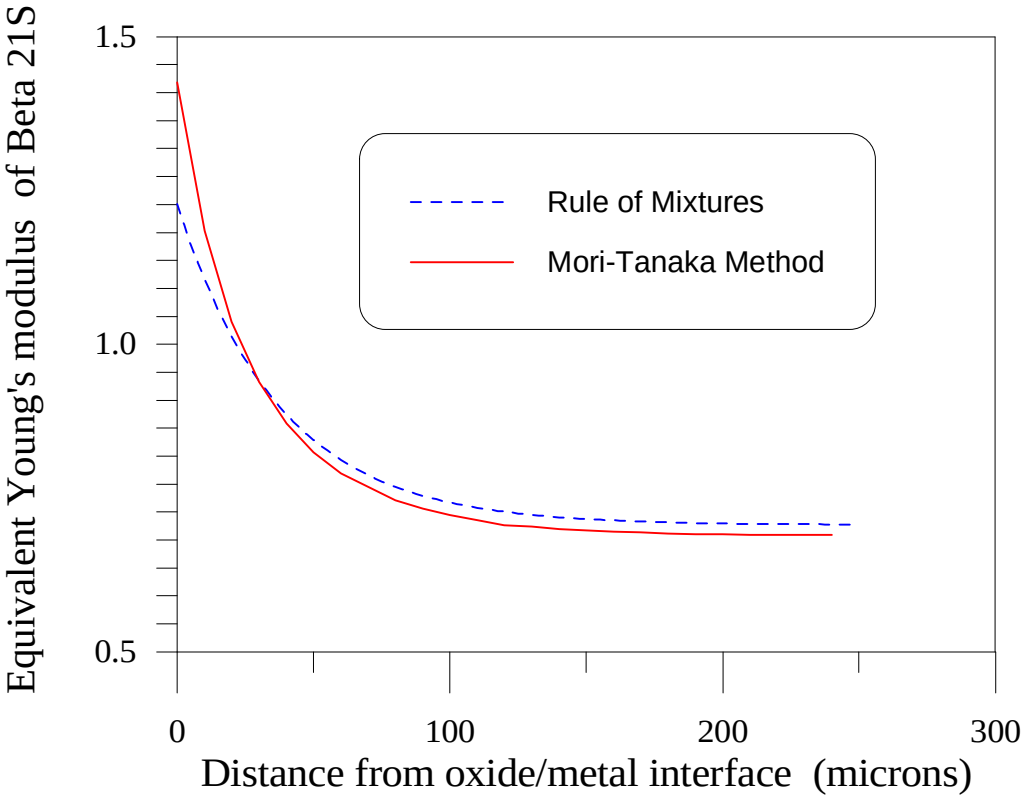

Fig.10 The effective Young's moduli of β-21S vs. position, evaluated by Mori-Tanaka method and the rule of mixtures.

Fig.11 Comparison of the normalized normal stress, $S_{11} = \sigma_{11} h / N_{11}$, between the uniform and gradient MMC cases ($x_1 = a$).

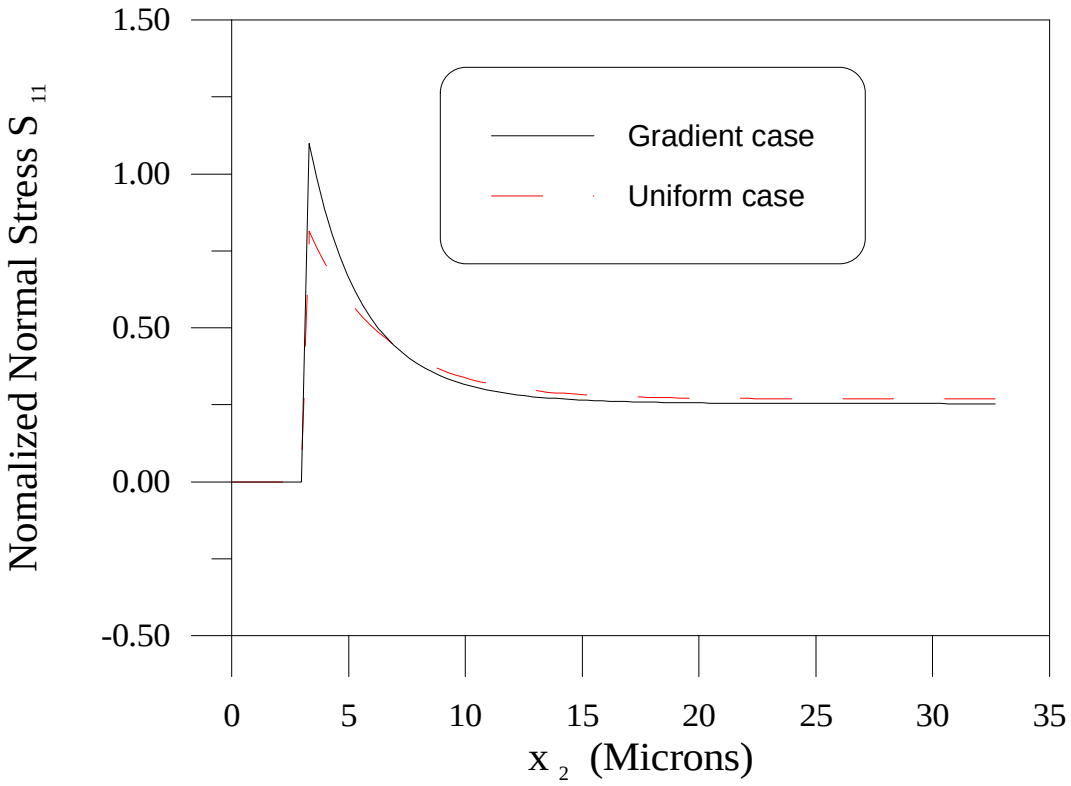

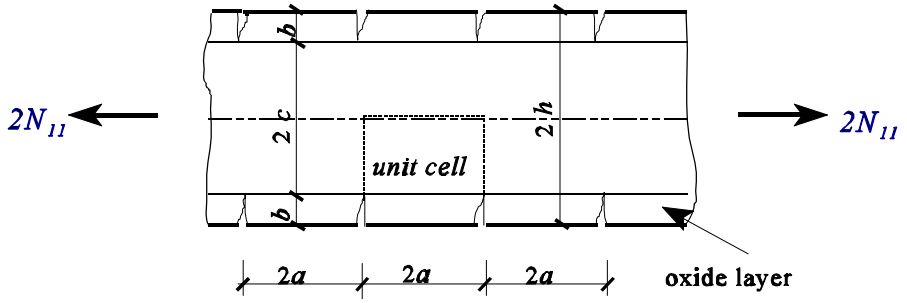

Fig.8 Microstructructureof β-21S oxidized at $700^0C$for 48 hrs.

(a)

(b)

Fig.2 (a) The Cross Section of the Oxidized MMC with Surface Cracks;
(b) The Represent Volume Element of the Model (RVE)

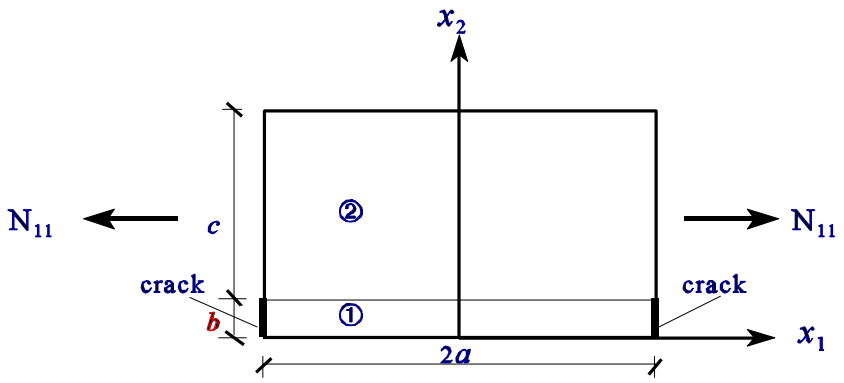

Fig.4(b) Normalized normal stress, $S_{11} = \sigma_{11} h/N_{11}$, on the surface of the oxide layer under the uniaxial load.

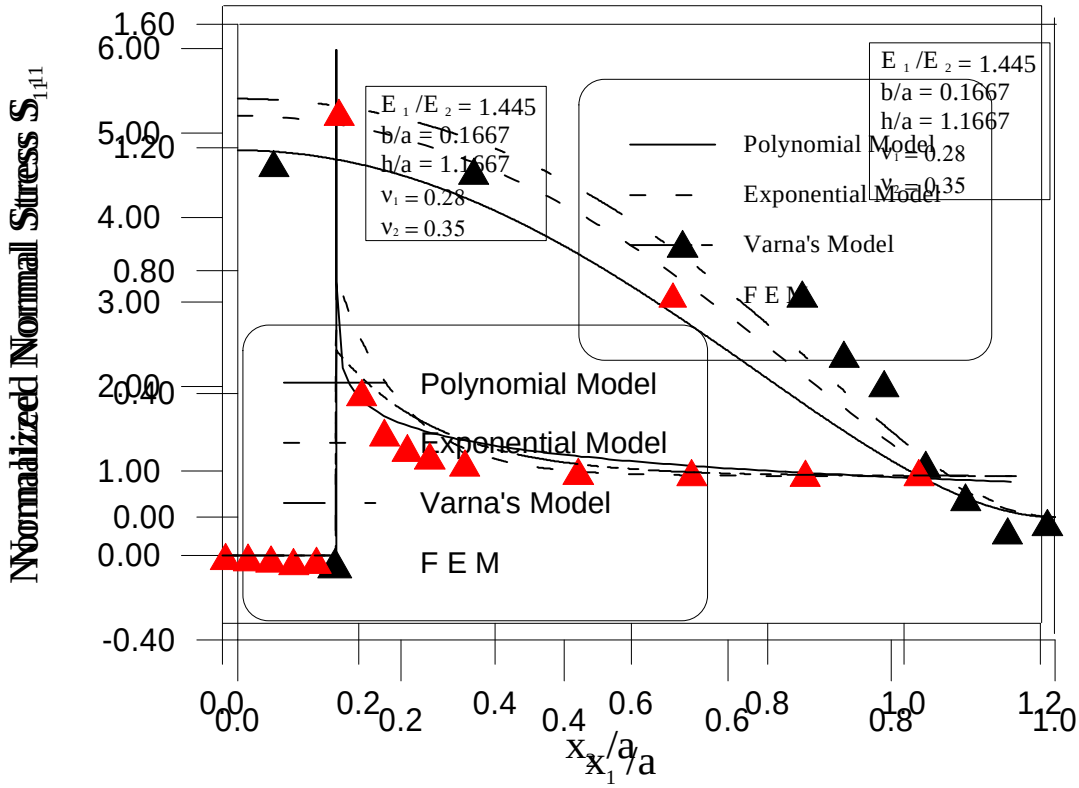

Fig.3(b) The normalized normal stress, $S_{11} = \sigma_{11} h/N_{11}$, through the thickness at $x_1 = a$ under uniaxial load.

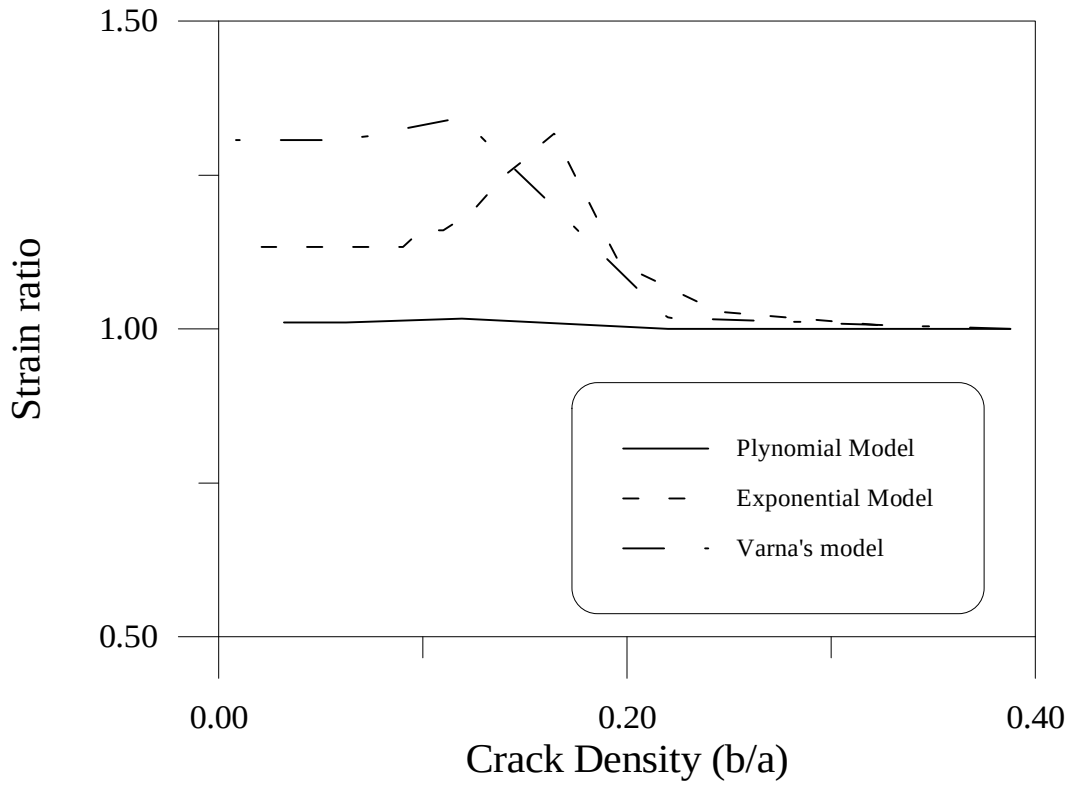

Fig. 6 The ratio of effective normal strain models between energy method and average method .

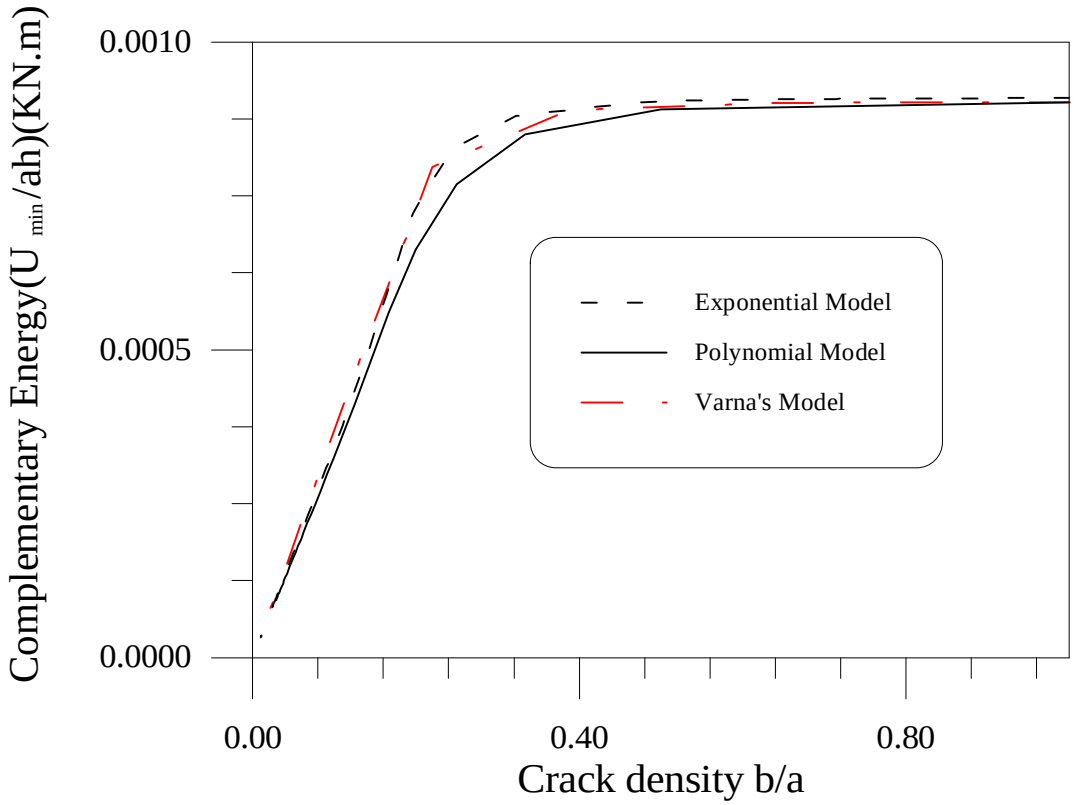

Fig.5. The comparing of minimum complementary energy given by the three types of test functions.